

EXPERIMENTAL DETERMINATION OF PYROXENE SOLVI FOR ≤ 1 KBAR AT 900 AND 1000° C

ALLAN C. TURNOCK

Department of Earth Sciences, The University of Manitoba, Winnipeg, Manitoba R3T 2N2

DONALD H. LINDSLEY

Department of Earth and Space Sciences, State University of New York,
Stony Brook, New York 11794, U.S.A.

ABSTRACT

Results of hydrothermal experiments at 900°C, $P = 1$ kbar (10^8 Pa) and dry experiments at 1000°, $P < 1$ bar (10^5 Pa) on synthetic pyroxenes in the system CaSiO_3 - MgSiO_3 - FeSiO_3 bracket equilibrium compositions of pyroxenes, pyroxenoids and fayalite + silica. Five tielines for coexisting augite + orthopyroxene at 900°C were determined; the locus of the compositions of the augite in equilibrium with orthopyroxene, A(O), is $X_{\text{Wo}}^{\text{A(O)}} = 42.5 (\pm 1.5) - 0.083 X_{\text{Fe}}^{\text{A(O)}} (X_{\text{Wo}} = \text{CaSiO}_3, \text{mol. \%}; X_{\text{Fe}} = 100\text{Fe}/(\text{Fe} + \text{Mg}), \text{atomic})$; the composition of orthopyroxenes O(A) is $X_{\text{Wo}}^{\text{O(A)}} = 2.3 + 0.03 X_{\text{Fe}}^{\text{O(A)}} (\pm 1.5)$. Both equations are valid for the range $8 < X_{\text{Fe}} < 60$. The A(O) solvus separates compositions of igneous (mafic) origin from those of crustal metamorphic origin. These results are not compatible with the geothermometers of Wood & Banno or of Wells. Pigeonite is present at these temperatures, but it has only a small range of compositions. The iron-rich corner of the subsolidus diagram shows the field of augite + olivine + silica.

Keywords: orthopyroxene, clinopyroxene, phase equilibria, geothermometry, ferrobustamite.

SOMMAIRE

Les résultats d'expériences hydrothermales (900°C, $P = 1$ kbar = 10^8 Pa) et à sec (1000°C, $P < 1$ bar = 10^5 Pa) sur pyroxènes synthétiques du système CaSiO_3 - MgSiO_3 - FeSiO_3 permettent de préciser les conditions d'équilibre de pyroxènes, de pyroxénoïdes et de fayalite + silice. On a déterminé la composition des phases dans cinq paires augite-orthopyroxène (A - O) en coexistence à 900°C. La composition de l'augite en équilibre avec l'orthopyroxène [A(O)] satisfait la relation $X_{\text{Wo}}^{\text{A(O)}} = 42.5 (\pm 1.5) - 0.083 X_{\text{Fe}}^{\text{A(O)}} (X_{\text{Wo}}$ est la proportion de CaSiO_3 en % molaire; $X_{\text{Fe}} = 100 \text{Fe}/(\text{Fe} + \text{Mg})$ en % atomique); celle de l'orthopyroxène en équilibre avec l'augite [O(A)] obéit à la relation $X_{\text{Wo}}^{\text{O(A)}} = 2.3 + 0.03 X_{\text{Fe}}^{\text{O(A)}} (\pm 1.5)$. Les deux expressions sont valides dans l'intervalle $8 < X_{\text{Fe}} < 60$. Le solvus A(O) sépare les pyroxènes d'origine ignée (roches mafiques) de ceux qui ont subi

un métamorphisme dans la croûte. Ces résultats ne concordent ni avec le géothermomètre de Wood & Banno, ni avec celui de Wells. La pigeonite n'est présente à ces températures que dans un domaine étroit de composition. L'assemblage augite + olivine + SiO_2 apparaît dans le coin riche en fer du diagramme subsolidus.

(Traduit par la Rédaction)

Mots-clés: orthopyroxène, clinopyroxène, équilibre de phases, géothermométrie, ferrobustamite.

DEFINITIONS AND ABBREVIATIONS

- A: Augite (Ca-rich Cpx; Cpx = clinopyroxene)
- O: Orthopyroxene
- P: Pigeonite (Ca-poor Cpx)
- F: Olivine + SiO_2 (approximately equimolar)
- B: Ferrobustamite
- A(Z): Augite saturated with phase Z; likewise for other phases. The locus of A(Z) compositions defines the *augite solvus*. Likewise, O(Z) defines the *orthopyroxene solvus*. We use "solvus" to mean "limit of solubility in a solid phase", not as a synonym for "miscibility gap".
- Di, Hd: the *components* $\text{CaMgSi}_2\text{O}_6$, $\text{CaFeSi}_2\text{O}_6$.
- Wo, En, Fs: the *components* CaSiO_3 , MgSiO_3 , FeSiO_3 .
- X_{Wo}^z , X_{En}^z , X_{Fs}^z : mole percentage of those components in phase Z.
- X_{Fe}^z : 100 Fe/(Fe + Mg) in phase Z; bulk ratio if superscript is omitted (different from X_{Fe}^z unless $X_{\text{Wo}}^z = 0$).

INTRODUCTION

This paper presents the results of the determination of the compositions of pyroxenes, fayalites and pyroxenoids that were synthesized and reacted to bracket equilibria. Five brackets on augite + orthopyroxene compositions define the A(O) and O(A) solvi at 900°C ($P=1$

kbar). Two brackets on augite + pigeonite were determined for 1000°C ($P < 1$ atm), and one was determined for 900°C. Complete brackets on one assemblage of augite + fayalite (+ silica) and partial brackets for another were obtained for 1000°C. One partial bracket was obtained for augite + ferrobustamite at 1000°C. These data are plotted on isothermal sections, which show subsolidus relations at 900° (1 kbar) and 1000°C (1 atm). These temperatures are greater than those of granulite-facies metamorphism, but lower than those of mafic igneous crystallization; thus they may be useful in the interpretation of these processes and in the distinction between them.

Knowledge of the approximate locations of the pyroxene solvi has accumulated over the years from the chemical analyses of those pyroxenes that are found coexisting in nature. The best examples are from cumulus igneous rocks (e.g., Skaergaard; Brown & Vincent 1963) and from metamorphic rocks in the granulite facies (e.g., Philpotts 1966, Davidson 1968) and in the pyroxene-hornfels facies (e.g., Simmons *et al.* 1974, Bonnichsen 1969). These data have been used to formulate T-X cross-sections of two-pyroxene solvus relationships (Hess 1941, Bonnichsen 1969) using temperature values taken from a knowledge of associated genetic processes.

Experimental calibration of the P-T-X variables of these solvi started with the work of Bowen *et al.* (1933), Bowen & Schairer (1935) and Atlas (1952) on three boundaries of the pyroxene quadrilateral (Hd-Fs, Fs-En and En-Di, respectively). After the refinement of the En-Di binary join by Boyd & Schairer (1964) and determination of the effect of pressure on the phase relationships (Davis & Boyd 1966), it was used as a geothermometer (Boyd 1973) for Mg-rich pyroxenes and also, by calculation (Wood & Banno 1973, Wells 1977), for iron-bearing pyroxenes. There are experimental determinations of solvi for compositions on the Hd-Fs join (at 20 kbar: Lindsley & Munoz 1969) and the iron-rich join $X_{Fe} = 85$ (at 15 kbar: Smith 1972). The augite-hypersthene solvi have been determined for compositions across the pyroxene quadrilateral for T = 810°C, P = 15 kbar by Lindsley *et al.* (1974), and for T = 1200°C at 15 and 30 kbar by Mori (1978). At lower pressures, 2 to 4 kbar, the solvi were investigated for temperatures of 700 to 800°C and bulk compositions on the join $X_{Fe} = 75$ by Simmons *et al.* (1974). Ross & Huebner (1979) gave polythermal data for coexisting augite-pigeonite-orthopyroxene. Many other experiments have been made on

Ca-Mg-Fe pyroxenes with other added components, such as Al_2O_3 . Results of these experiments, mainly at high pressures and mostly of the synthesis type, are not directly comparable with the results of our study.

EXPERIMENTAL

The method of Lindsley *et al.* (1974), which brackets equilibrium compositions of Ca, Mg and Fe by exchange or exsolution reactions, was used.

Starting materials

The reactants were synthetic Ca-Mg-Fe pyroxenes, made by the methods of Turnock *et al.* (1973). These crystalline powders had a grain size of 5 to 50 μm ; the larger grains were aggregates of crystals or, rarely, single crystals. The process included several cycles of heating and grinding. The margins of the crystals were cleavage faces at the edges, caused by grinding, or anhedral growth boundaries against another crystal. The homogeneity of these grains was tested by the electron-microprobe analysis of 20 grains in each of 3 clinopyroxene preparations; the scatter of points indicates that there is a variation in composition of approximately 5% in the range of values for the components En, Fs and Wo. This inhomogeneity reflects zoning of unknown geometry but on the scale of the probe-beam spot size (1 μm). Chemical impurities are those of the reagent-grade chemicals (principally Na, < 0.03 wt. %); also, Al_2O_3 was added to some samples from an Al_2O_3 mortar during grinding. The maximum amount of Al_2O_3 , 1 wt. %, was found in an iron-rich preparation ($X_{Fe} = 60$, $X_{Wo} = 10$) that had been ground 20 times. Other samples with $X_{Fe} < 60$ required considerably less grinding; none has more than 0.3 wt. % Al_2O_3 . All samples with $X_{Fe} > 60$ were ground in an agate mortar and thus gained no Al_2O_3 .

The compositions of the reactants for each experiment are listed in Table 1. For experiments at 900°C, water was an additional component; 3 mg H_2O was added to 25 mg pyroxene and sealed in a capsule of Ag-Pd alloy. The presence of H_2O appeared to catalyze the reactions; it did not lead to the formation of hydrates. For experiments at 1000°C, pyroxene powders were tamped into iron capsules, an iron lid was crimped on, and these were placed inside a silica-glass capsule that was then sealed under vacuum.

Seeding was necessary to nucleate orthopyroxene in order to start its recrystallization from

TABLE 1. LIST OF EXPERIMENTS

No.	Reactants	Crucible	T, °C	Pressure bars	Time hrs.	Products		No.	Reactants	Crucible	T, °C	Pressure bars	Time hrs.	Products	
						Probe	XRD							Probe	XRD
100Fe/(Fe+Mg) = 10, X _{Wo} = 30															
8	A+seeds 0	AgPd	900	1000	528	Fig. 1a	A(9,42)+0	4	A	Fe	1000	<1	5520	Fig. 2d	A(-,33)+P(-,15)+F
9	A(0,46)+0(20,0)	AgPd	900	1000	528	Fig. 1b	A(5,43)+0	4	A(60,40)+P(60,10)	Fe	1000	<1	5520	Fig. 2d	A(-,37)+P(-,11)+F
10	A(20,50)+0(3,0)	AgPd	900	1000	528	Fig. 1c	A(10,41)+0	5	A(30,40)+P(75,10)+0	Fe	1000	<1	5520	Fig. 2e	A(-,37)+P(-,14)+F
100Fe/(Fe+Mg) = 20, X _{Wo} = 30															
1	A+seeds 0	AgPd	900	1000	528	Fig. 1d	A(18,37-40)+0								
100Fe/(Fe+Mg) = 20, X _{Wo} = 25															
14	A(0,50)+0(30,0)	AgPd	900	1000	528	Fig. 1e	A(-,42-47)+0	5	A	Fe	1000	<1	5520	Fig. 2b	P(-,14)+A(-,32-35)+F
15	A(20,50)+0(20,0)	AgPd	900	1000	528	Fig. 1f	A(-,40-46)+0	6	A(60,40)+0(60,0)	Fe	1000	<1	5520	Fig. 2f	P(-,13)+A(-,39)
1	A(20,50)+0(20,0)	Fe	1000	<1	5520		A(-,49)+0+F	7	A(30,40)+0(75,5)	Fe	1000	<1	5520	Fig. 2f	P(-,12)+A(-,35)+F
2	A(0,50)+0(30,0)	Fe	1000	<1	5520		A(-,47)+0+F								
100Fe/(Fe+Mg) = 20, X _{Wo} = 20															
S28	A	Fe	1000	<1	5520		A(-,32)+P(-,12)+F	11	A	Fe	1000	<1	5520		A(-,37)+F+S
100Fe/(Fe+Mg) = 30, X _{Wo} = 30															
10	A	Fe	1000	<1	5520		A(30,33)	9	A	Fe	1000	<1	5520		A(-,32)+S
11	A(30,50)+P(30,5)	Fe	1000	<1	5520		A(-,37-43)+P(-,~13)+F								
12	A(0,50)+P(50,4)	Fe	1000	<1	5520		A(-,39-43)+P(-,~15)+F								
13	A(30,50)+0(30,5)	Fe	1000	<1	5520		A(-,37-46)+P(-,~15)+F								
27	A(30,50)+0(30,5)	AgPd	900	1000	528	Fig. 1g	A(25,43)+0	88	A(75,45)+P(75,10)+0	Fe	1000	<1	5520	Fig. 2g	A(-,33)+S+F
28	A(0,50)+P(50,4)	AgPd	900	1000	528	Fig. 1h	A(-,41)+0	89	A	Fe	1000	<1	5520	Fig. 2g	A(-,32)+S+F
29	A+seeds 0	AgPd	900	1000	528	Fig. 1i	A(-,37)+0	90	A(60,40)+P(85,10)	Fe	1000	<1	5520	Fig. 2h	A(-,33)+S+F
100Fe/(Fe+Mg) = 40, X _{Wo} = 25															
7	A(30,40)+0(50,0)	AgPd	900	1000	840	Fig. 1j	A(-,~35)+0	91	A(75,50)+0(75,0)	Fe	1000	<1	5520	Fig. 2h	A(-,35)+S+F
8	A(50,40)+0(30,0)	AgPd	900	1000	840	Fig. 1k	A(-,~37)+0	92	A(85,25)+P(60,25)	Fe	1000	<1	5520	Fig. 2i	A(-,32-39)+S+F
9	A+seeds 0	AgPd	900	1000	966	Fig. 1l	A(-,30-40)+0+P	93	A(100,40)+P(60,10)	Fe	1000	<1	5520	Fig. 2j	A(-,34)+S+F
100Fe/(Fe+Mg) = 50, X _{Wo} = 30															
6	A	Fe	1000	<1	5520	Fig. 2a	A(-,31)+S	94	A(50,40)+F+S	Fe	1000	<1	5520	Fig. 2j	A(-,35)+S+F
7	A(50,50)+P(50,4)	Fe	1000	<1	5520	Fig. 2a	A(-,35-44)+P(-,15)+S								
8	A(30,50)+P(60,10)	Fe	1000	<1	5520	Fig. 2b	A(-,37)+P(-,13)+S								
13	A+seeds 0	AgPd	900	1000	966	Fig. 1m	A(-,34-38)+P								
14	A(50,50)+P(50,4)	AgPd	900	1000	966	Fig. 1n	A(-,35-39)+P(-,7-11)								
100Fe/(Fe+Mg) = 50, X _{Wo} = 25															
5	A(30,50)+0(60,0)	Fe	1000	<1	5520	Fig. 2c	A(-,39-42)+P(-,12)								
7	A(30,50)+0(60,0)	AgPd	900	1000	840	Fig. 1o	A(45,39-42)+0								

A = augite, 0 = orthopyroxene, P = pigeonite, B = ferrobustamite, F = olivine, S = silica. Compositions in brackets after letter which designates phase, e.g. A(60,40) means: 60=100Fe/(Fe+Mg), 40=X_{Wo} mol %, - means analysis not possible.

clinopyroxene, especially in the dry experiments at 1000°C. Synthetic orthopyroxene, or mechanical mixtures of synthetic orthopyroxene + clinopyroxene with appropriate bulk composition, was added to orthopyroxene-free reactants in amounts of 1 to 2%. This seeding complicated the interpretation of results, as discussed below.

Experimental conditions

Experiments at 900°C were performed in hydrothermal apparatus with $T \pm 5^\circ$, $P = 1000 \pm 20$ bars (1 bar = 10^5 Pa), with $f(O)_2$ controlled near the iron-wüstite equilibrium values by the graphite-methane buffer (Huebner 1971).

Experiments at 1000 \pm 5°C were of the dry-heating type, in evacuated silica-glass capsules with $P < 1$ bar. The internal iron containers had a metallic lustre at the start of the experiment and a dark tarnish at the end of the experiment; therefore, they appeared to have controlled $f(O)_2$ at the iron-wüstite buffer.

For hydrothermal experiments, cooling was done by an air-blowing quench, which lowered the temperature to less than 300°C in 3–5 minutes. The evacuated silica-glass tubes were quenched in cold water; the Fe capsules were cooled below red heat in several seconds.

Analysis of products

X-ray diffraction (XRD) and electron-microprobe analysis were used to characterize the crystalline phases in the run products. X-ray diffraction traces were recorded over the range 20 to 50° 2 θ , using Cu K α radiation. The (220), (22 $\bar{1}$) (310), (31 $\bar{1}$), (221) and (311) reflections were used to derive Ca contents of the clinopyroxenes utilizing the relationships of Turnock *et al.* (1973). The error in the determination is estimated at $\pm 3\%$ Wo for patterns with sharp peaks; however, most of the patterns had irregular peaks (scatter of composition) and therefore larger errors. A few sharp patterns also yield values of X_{Fe} from measurements of the (150) reflection; estimated error is ± 4 . Results are listed in Table 1.

Electron-microprobe analysis was done on grain mounts, using the methods and standards of Lindsley & Dixon (1976). The Fe standard was Rockport fayalite. Fe/Mg ratios were monitored by means of a synthetic orthopyroxene. Grains were broken from the lump product in a mortar and pestle, giving grains of 4 to 25 μ m; however, most of the larger grains are aggregates of crystals whose maximum lengths rarely exceed 10 μ m. We did not discover the contamination of some of our starting

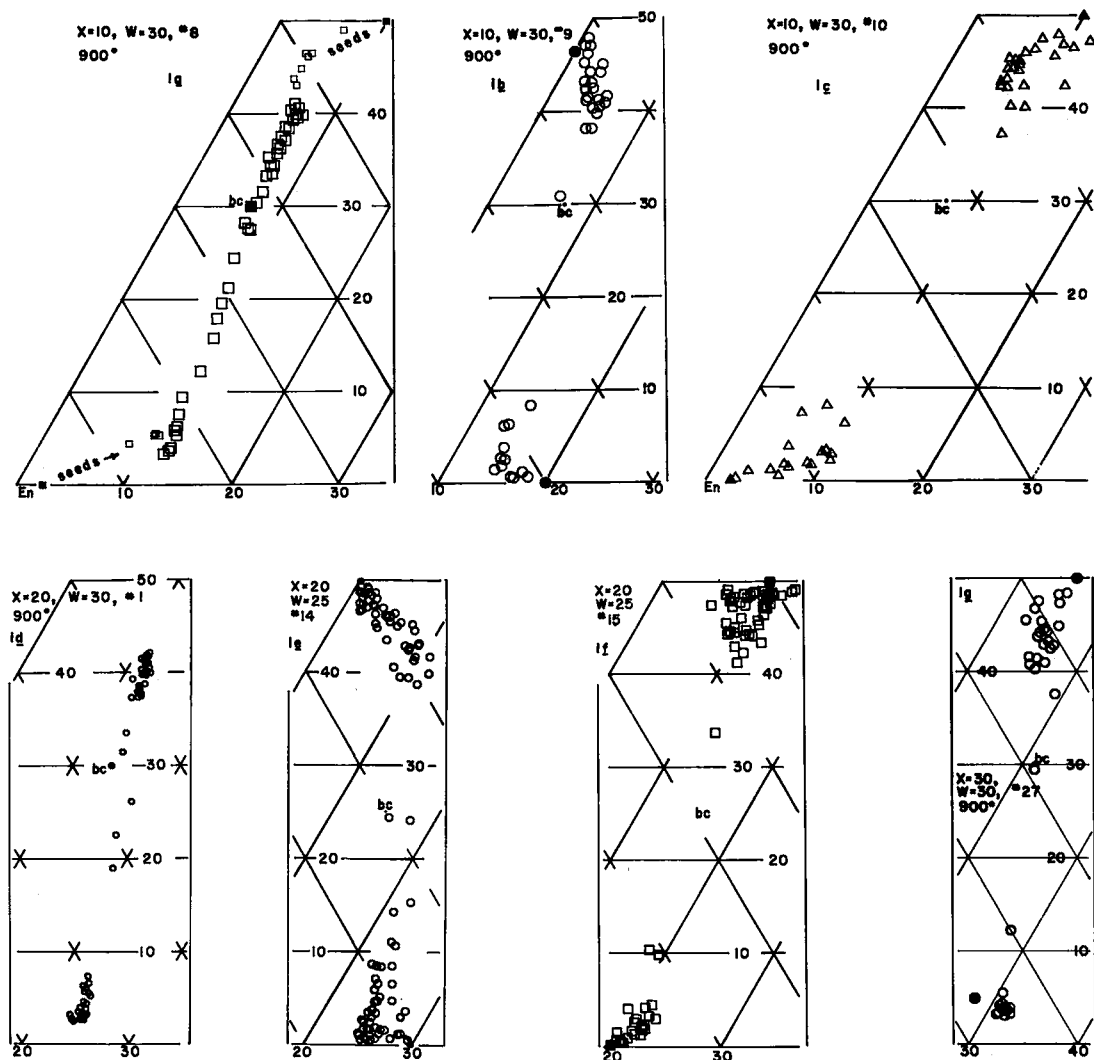


FIG. 1. Electron-microprobe analytical points plotted in the pyroxene quadrilateral of the system En-Fs-Wo (MgSiO_3 - FeSiO_3 - CaSiO_3 , mol. %). Each set of experiments is labeled by bulk composition (given as $X_{\text{Fe}} = 100 \text{ Fe}/(\text{Fe}+\text{Mg})$, $W = X_{\text{Wo}} = \text{CaSiO}_3$ mol. %), a sequence number and the temperature (900°C). Circles, triangles and squares = probe analysis. Solid symbols: compositions of reactant. Point bc: bulk composition of reactants.

materials with Al_2O_3 until the analysis of run products was completed. Accordingly, our analyses were restricted to CaO, MgO, FeO and SiO_2 . Analyses were accepted if they (1) had sums between 96 and 102 wt. % and (2) showed between 3.98 and 4.02 cations *per* six oxygens. The results are shown in Figures 1 and 2.

INTERPRETATION

The probe-analysis points, with the aid of

the XRD determinations, are interpreted in terms of reaction paths, zoned or lamellar crystals and the fact that the excitation volume of the beam may overlap crystal boundaries and give a composite analysis. The reaction path can be discerned in the scatter of points in most of the diagrams of Figures 1 and 2. One exception is shown in Figure 1m, which does not show a path nor a concentration of points at the exsolution compositions given by XRD. More difficult than interpreting the path of

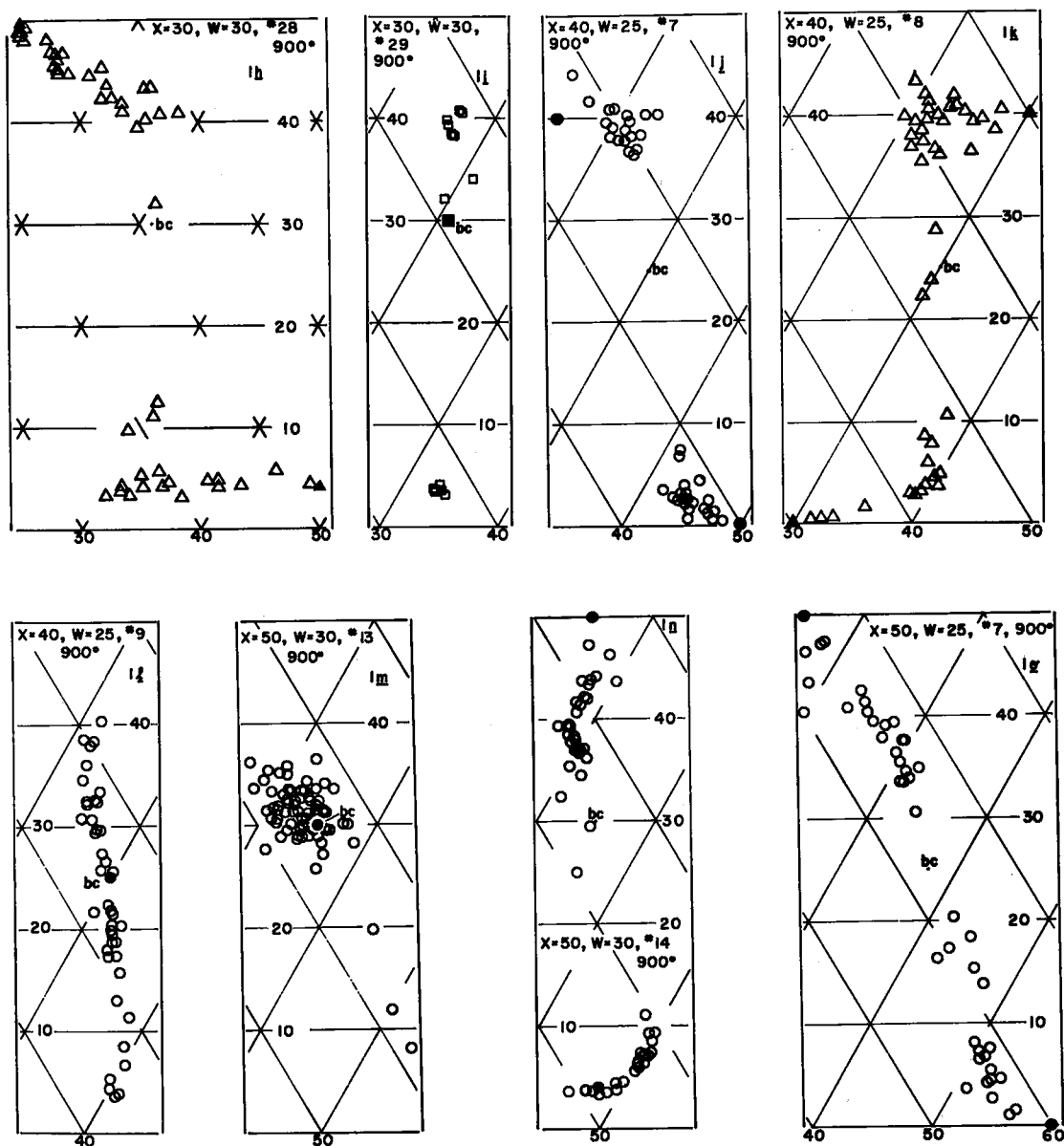


FIG. 1. Electron-microprobe analytical points of products of experiments at 900°C (continued).

reaction is recognizing the maximum amount of reaction, which is obscured by grain-overlapped points. We give our best estimates as arrows in Figure 3.

Figure 1a shows the probe-data points for exsolution from composition $X_{Fe} = 10$, $X_{w_0} = 30$. Most of the composition points lie along a tieline between compositions of minimum and maximum exsolution reaction. The intermediate

points along this tieline are interpreted to be the result of the electron beam encompassing several exsolution lamellae within a crystal, or the beam overlapping a boundary and including parts of two crystals. Those points that do not lie on this line, or that form an unexpected extension of it, are marked by symbols of a smaller size; these points are interpreted as zoned overgrowths on the seeds

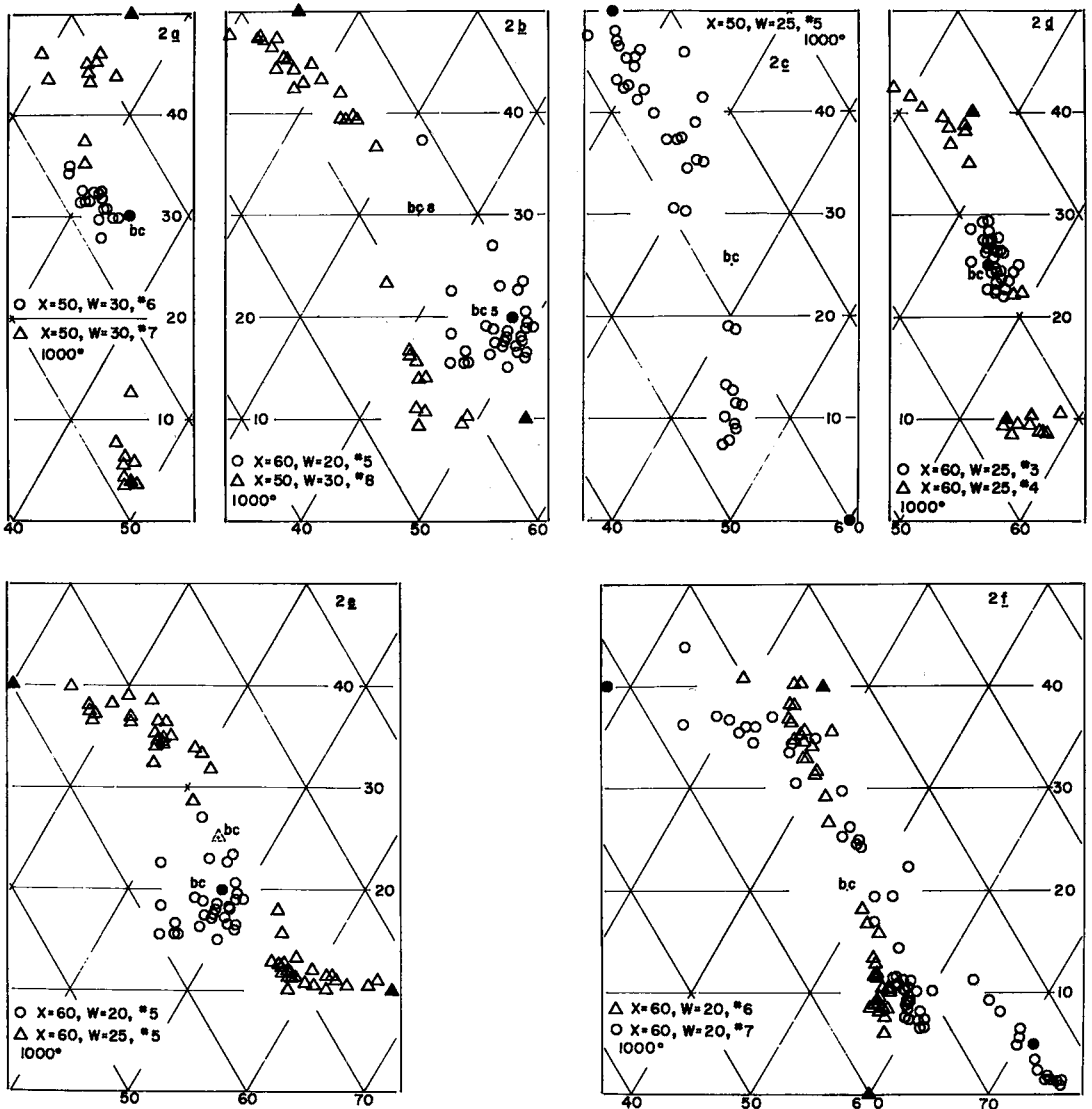


FIG. 2. Electron-microprobe analytical points of products of experiments at 1000°C. Symbols as in Figure 1.

(orthopyroxene $X_{\text{Fe}^0} = 3$, $X_{\text{W}0} = 0$, plus clinopyroxene $X_{\text{Fe}^A} = 20$, $X_{\text{W}0^A} = 50$). The calcium content of the product clinopyroxene, as determined by the XRD method, is $X_{\text{W}0} = 42$ (Table 1), and the relative sharpness of the peaks in the XRD pattern indicates that the clinopyroxene crystals are predominantly of this composition. Therefore, the intermediate compositions indicated by the probe points result mainly from overlap of grain boundaries within the excitation volume of the beam. A similar interpretation is given to probe points intermediate be-

tween the starting composition and the orthopyroxene. The composition of the product orthopyroxene is taken to be $X_{\text{Fe}^0} = 13$, $X_{\text{W}0} = 4$ from the position of probe points at the extremity of the line of points; a more calcic composition is not expected. Therefore, the intermediate compositions obtained by microprobe can be interpreted as the result of beam overlap on intergrowths of the clinopyroxene and the orthopyroxene. These interpretations of the reaction paths are shown by arrows in Figure 3. The point of each arrow gives the composi-

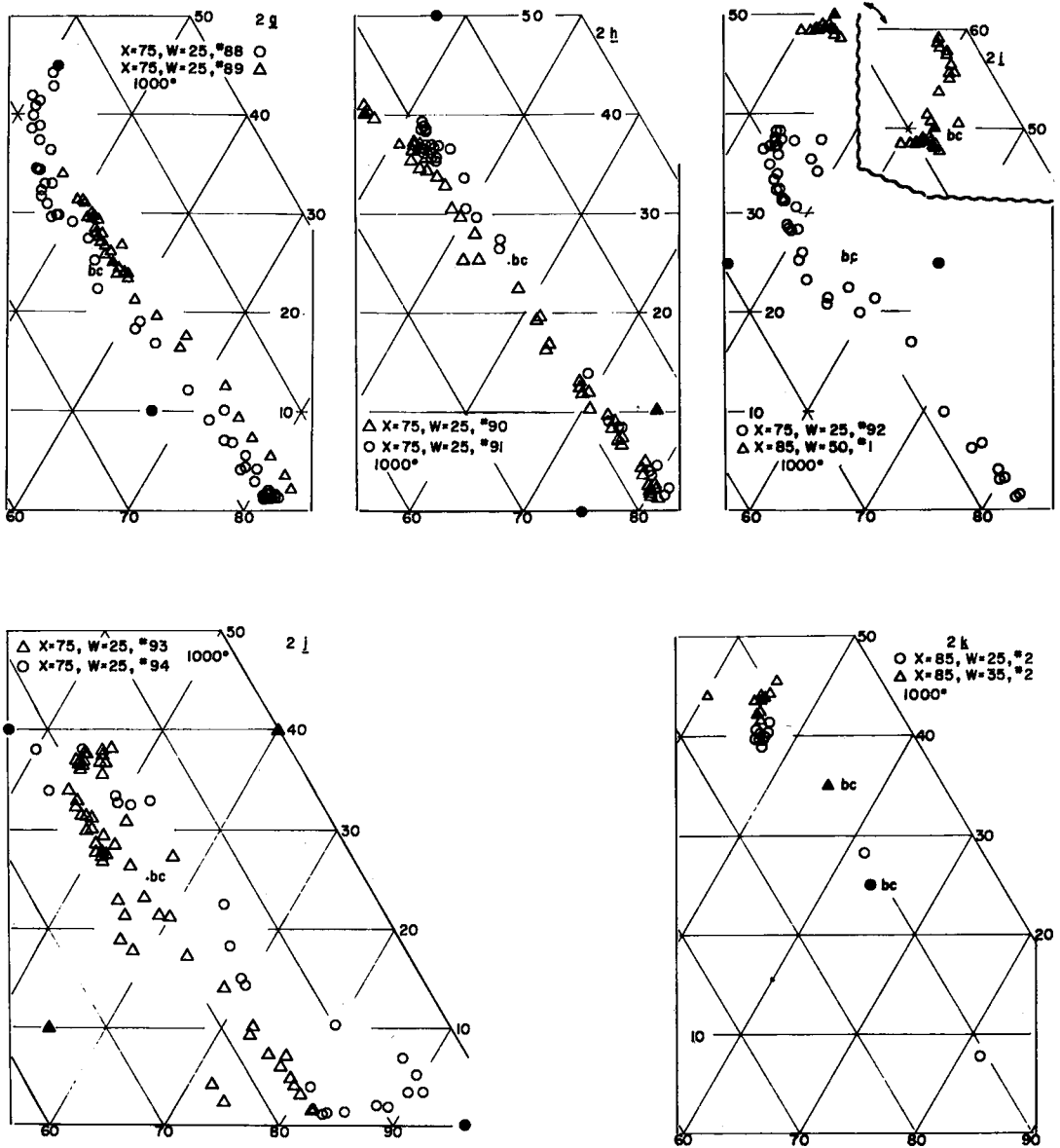


FIG. 2. Electron-microprobe analytical points of products of experiments at 1000°C (continued).

tion of the product and the direction in which it is approaching equilibrium.

Figure 1b shows the probe-derived analytical data on the products of an experiment in which a mechanical mixture of clinopyroxene and orthopyroxene were reacted. The trends of the points indicate that the clinopyroxene lost calcium and gained iron, whereas the orthopyroxene lost iron and gained calcium. The occurrence of probe compositions near that of the

clinopyroxene starting material indicates that there is unreacted material, probably in the cores of crystals. This zoning, indicated by the points as $X_{w_o}^A$ 47 to 40, was poorly defined by the XRD method, which gave $X_{w_o}^A = 43$ on broad peaks. The composition of maximum reaction, using the two methods, is estimated to be $X_{w_o}^A = 42 \pm 2$.

The trend of points of orthopyroxene in Figure 1b shows a reaction path from the original

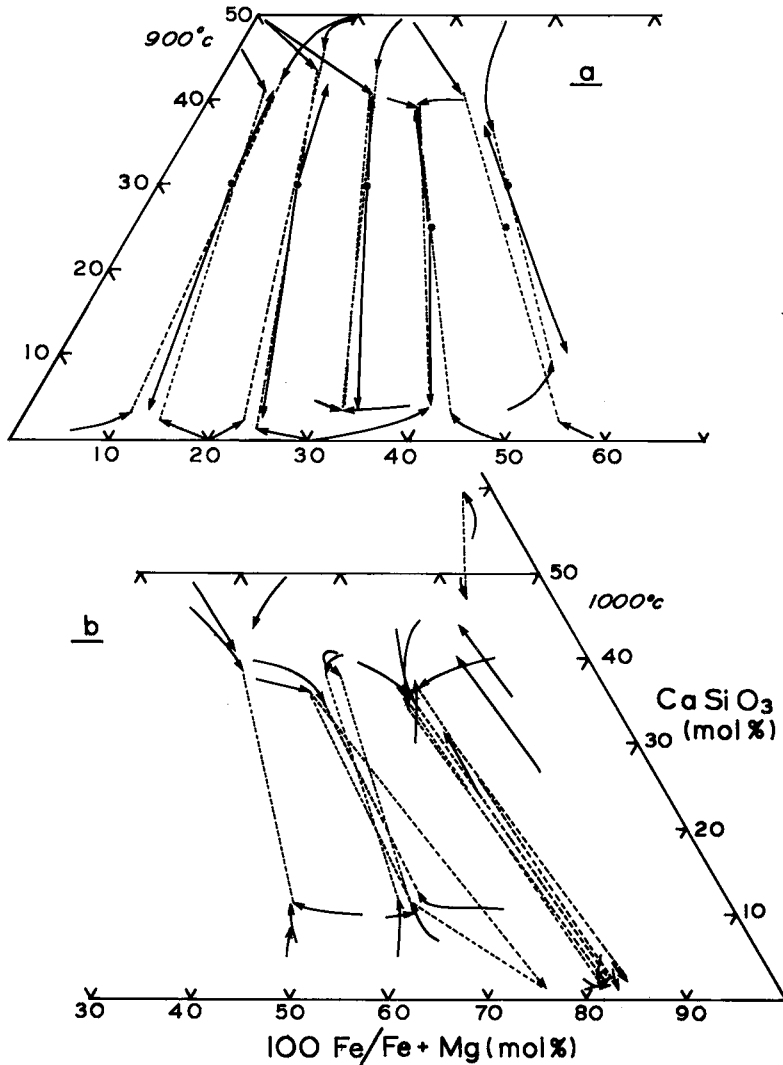


FIG. 3. Experimental reactions of solid-solution exchange, and exsolution. (a) 900°C. (b) 1000°C. Solid lines: reaction paths. Dashed lines: product tielines.

composition to a cluster of points at $X_{Fe}^0 = 15$, $X_{wo}^0 = 2$; this is interpreted as zoning. There are also three points with greater contents of Ca that are interpreted as the result of overlap of the probe beam on adjacent crystals of orthopyroxene and clinopyroxene. The interpreted paths of reaction are shown in Figure 3.

In a number of attempted exsolution-experiments, especially at 1000°C (dry), the intermediate single-phase clinopyroxenes either persisted metastably or broke down into such fine-grained intergrowths that they could barely be

resolved, or not at all, by electron microprobe. We include these experiments where the XRD analysis shows that exsolution did, in fact, take place.

The data for $X_{Fe} = 50$ at 900°C (Figs. 1m-1o) show inconsistencies caused by metastable nucleation in exsolution and metastable persistence. A single-phase clinopyroxene (Wo₃₀, #13, Table 1) exsolved to augite plus pigeonite despite the presence of orthopyroxene seeds. Likewise, #14, a mechanical mixture of augite and clinopyroxene (Wo₄) without orthopyroxene

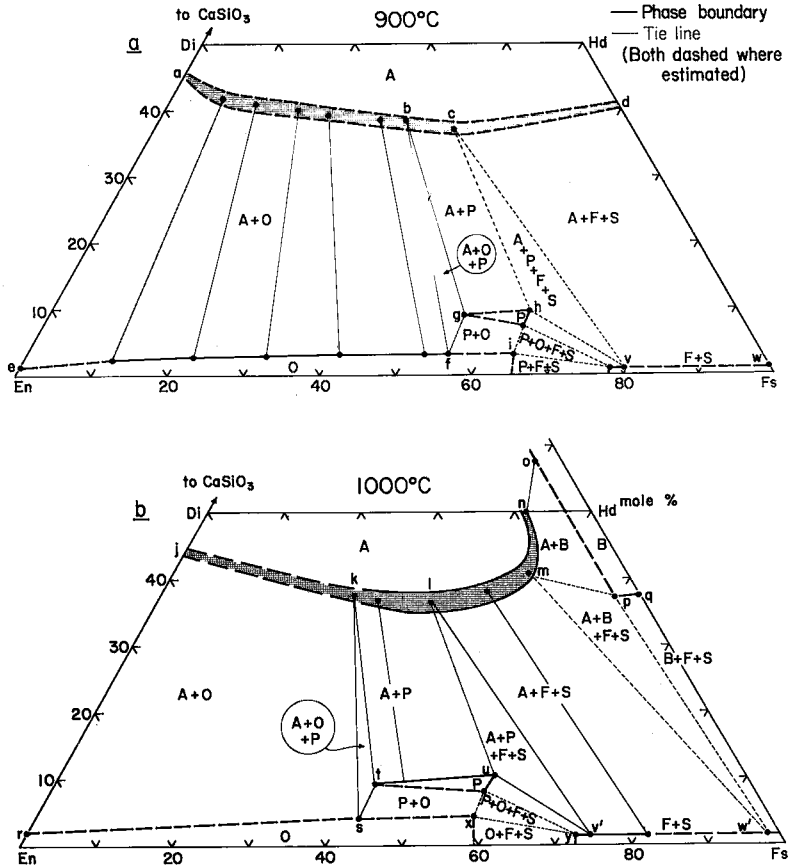


FIG. 4. Subsolidus diagrams of the pyroxene quadrilateral (a) at 900°C, 1 kbar and (b) at 1000°C, < 1 atm. Abbreviations as in Table 1. The three-pyroxene triangles are from Podpora & Lindsley (1979).

seeds, produced augite plus pigeonite. By contrast, orthopyroxene in #17 gained Ca and Mg but did not convert to pigeonite. Podpora & Lindsley (1979) have shown that the most Mg-rich pigeonite stable at 900°C occurs at approximately $X_{Fe} = 60$; accordingly, we interpret the pigeonites in experiments 13 and 14 as metastable, and show orthopyroxene as the stable low-calcium phase at $X_{Fe} = 50$ in Figure 4a.

For other experiments listed in Table 1, and on the basis of probe data as shown in Figures 1 and 2, a similar interpretation leads to the arrows shown in Figure 3; these arrows limit the position of the solvi as indicated in Figure 4. It is clear from Figures 1, 2 and 3 that our experimental brackets of the A(O) solvi yield considerable uncertainty in $X_{wo}^{A(O)}$. Some of this scatter is doubtless due to analytical error, but

we suggest that much of it is due to a gentle curvature of the Gibbs free-energy surface for augite, so that variations of 1 to 3 mole % W_o have but a minor effect on the free energy and thus also on the driving force for further reaction.

Presumably the failure of the cores of many grains to reach equilibrium is controlled mainly by the rate of diffusion of Ca, Mg and Fe in the solids; our experiments may carry much information on diffusion rates. The very small size of most product crystals (4–10 μm) precludes the determination of diffusion profiles on individual grains; the trends shown in Figures 1 and 2 reflect analyses of many individual grains. Since we did not do rate studies, our results can only put upper limits on diffusion rates.

THE SUBSIDUS PHASE DIAGRAMS

The field of solid solution of augite (marked A in Fig. 4) extends from the Di-Hd join to the A(Z) solvus at lower contents of calcium. This lower boundary at 900°C is the solvus *a-b-c-d* (Fig. 4a), and at 1000°C it is *j-k-l-m-n* (Fig. 4b). The portion of the solvus A(O) that has been experimentally determined by the reaction arrows of Figure 3a is listed in Table 2 and is shown by a stippled band in Figure 4a to emphasize the experimental uncertainty in $X_{\text{wo}}^{\text{A(O)}}$. An approximate equation of the band in the region $8 < X_{\text{Fe}} < 60$ is $X_{\text{wo}}^{\text{A(O)}} = 42.5 (\pm 1.5) - 0.083 X_{\text{Fe}}^{\text{A(O)}} (900^\circ\text{C}, 1 \text{ kbar})$. This equation can be extrapolated to $X_{\text{wo}}^{\text{Dl}} = 42.5$ on the Di-En join, a composition that is less calcic than has been determined for that join [cf., $X_{\text{wo}}^{\text{Dl}} = 48.2$; Boyd & Schairer (1964), 44.3 (extrapolated from high-pressure data): Lindsley & Dixon (1976)]. Thus the band must curve in the region $0 < X_{\text{Fe}} < 8$. For the Fe-free termination (point *a*, Fig. 4a), we

have used the value $X_{\text{wo}}^{\text{Dl}} = 45.5$ calculated for 900°C, 1 kbar from the solution model of Lindsley *et al.* (1981).

The O(A) solvus for 900°C, 1 kbar (line *e-f-i* in Fig. 4a) may be curved as shown, although the data permit a straight line. Point *e* is calculated from the solution model of Lindsley *et al.* (1981). The composition of orthopyroxene coexisting with augite [O(A)] at 900°C can be expressed as $X_{\text{wo}}^{\text{O(A)}} = 2.3 (\pm 0.5) + 0.03 X_{\text{Fe}}^{\text{O(A)}}$ for $8 < X_{\text{Fe}} < 60$. Compositions on this line, at the intersection of the best tielines (shown in Fig. 4a), are given in Table 2.

The three-pyroxene triangle *b-f-g* is from Podpora & Lindsley (1979, unpubl. data). This triangle should have been most affected by Al_2O_3 , inasmuch as the $X_{\text{Fe}} = 60$ starting materials used by Podpora & Lindsley (1979) prove to be those containing approximately 1 wt. % Al_2O_3 , but new experiments on Al_2O_3 -free starting phases indicate no significant differences within the combined experimental and analytical uncertainties. The solvus *f-i* was not determined.

The field of augite (A) extends to the boundary Hd-Fs at 900°C (Fig. 4a). The composition of point *d*, the augite richest in iron, is taken from Lindsley & Munoz (1969), as is point *w*. Other phase relations for $X_{\text{Fe}} > 60$ in Figure 4a (points *c, h, i, v*) are inferred from natural occurrences and from experiments at other pressures and temperatures.

The phase diagram for 1000°C, 1 atm (Fig. 4b) is complicated by the existence of ferrobustamite at compositions near $\text{CaFeSi}_2\text{O}_8$. The augite solvus (band *j-k-l-m-n*) reflects the coexistence of augite with a variety of phases and assemblages: *j-k*, A(O); *k-l*, A(P); *l-m*, A(F + S); *m-n*, A(B). Points *j* and *r* (Fig. 4b) are calculated from the model of Lindsley *et al.* (1981). Mixtures in the range $0 < X_{\text{Fe}} < 40$ at 1000°C did not react sufficiently to permit determination of the solvi *j-k* and *r-s*; these are inferred and, hence, are shown with dashed lines. The three-pyroxene triangle *k-s-t* was obtained by interpolation between the results of Podpora & Lindsley (unpubl. data): their three-pyroxene triangle falls at $1040 \pm 15^\circ\text{C}$ for $X_{\text{Fe}} = 40$ and at $970 \pm 15^\circ\text{C}$ for $X_{\text{Fe}} = 50$.

Point *l* in Figure 4b is A(P,F,S); it is placed at $X_{\text{Fe}} = 56 \pm 2$, $\text{Wo} = 36.5 \pm 2$ from the data in Figure 3b. Point *m*, which is A(B,F,S), is placed in Figure 4b at $X_{\text{Fe}} = 79 \pm 3$, $\text{Wo} = 41 \pm 3$. The calcium content is that given by XRD (Table 1, $X_{\text{Fe}} = 85$, $\text{Wo} = 35$, #2) even though some greater contents are given by probe determinations (Fig. 2k). The lower value is also preferred by reference to Huebner & Turnock (1980, their Fig. 3f), who show that

TABLE 2. INTERPRETED COMPOSITIONS OF COEXISTING PHASES, AND CALCULATED TEMPERATURES

$T_{\text{exp}}^{\circ}\text{C}$	X_{wo}^{A}	X_{En}^{A}	X_{Fs}^{A}	X_{wo}^{Z}	X_{En}^{Z}	X_{Fs}^{Z}	$X_{\text{D}}^{\text{Fe-Mg}}$	$T_{\text{WB}}^{\circ}\text{C}$	$T_{\text{W}}^{\circ}\text{C}$	K_{WB}
Z = Opx										
900	40.5	52.5	7.0	2.3	84.7	13.0	0.856 ^{+0.011}	1158	1123	0.206
	43.5	50.0	6.5				-0.181	1087	1030	0.142
900	39.5	49.0	11.5	3.0	74.0	23.0	0.754 ^{+0.044}	1074	1109	0.252
	42.5	47.0	11.0				-0.140	1017	1027	0.180
900	39.0	43.0	18.0	3.2	63.8	33.3	0.788 ^{+0.117}	990	1062	0.271
	42.0	41.3	16.7				-0.065	945	993	0.201
900	38.5	39.3	22.2	3.3	55.7	41.0	0.764 ^{+0.119}	949	1043	0.309
	41.5	38.0	20.5				-0.025	911	962	0.236
900	37.5	33.0	29.5	3.4	44.3	52.3	0.750 ^{+0.081}	908	1012	0.356
	40.5	31.7	27.8				-0.075	874	957	0.275
900	37.0	29.5	33.5	3.5	40.0	56.5	0.790 ^{+0.165}	889	989	0.357
	40.0	28.6	31.4				-0.066	860	942	0.284
1000	36.5	37.7	25.8	4.2	53.4	42.4	0.846 ^{+0.097}	953	1054	0.334
	39.5	36.4	24.1				-0.072	921	1002	0.267
Z = Ptg										
900	37.0	29.5	33.5	9.5	36.3	54.2	0.748 ^{+0.079}		(1028)	0.437
	40.0	28.6	31.4				-0.061		(977)	0.349
1000	36.5	37.7	25.8	9.5	49.2	41.4	0.796 ^{+0.062}		(1091)	0.402
	39.5	36.4	24.1				-0.040		(1034)	0.318
1000	36.0	35.0	29.0						(1073)	0.418
	39.0	33.7	27.3	9.5	45.0	45.5	0.810 ^{+0.078}		(1021)	0.335
							-0.070			
1000	36.0	28.0	37.0	10.5	32.5	57	0.732 ^{+0.070}		(1053)	0.534
	38.0	27.6	34.4				-0.061		(1016)	0.457
Z = Olivine + Sil ₂ O ₂										
1000	35.6	27.7	36.7	1.3	24.5	74.2	0.430 ^{±0.050}			
	37.5	27.5	35.0							
1000	37.3	19.5	43.2	1.3	17.0	81.7	0.449 ^{±0.050}			
	38.7	19.7	41.4							
Z = Ferrobustamite										
1000	50.0	8.4	41.6	58.0	3.4	38.6	0.436 ^{±0.040}			

exp. = experimental

X = mol %. F = olivine-silica projection onto pyroxene quadrilateral.

 $K_{\text{D}}^{\text{Fe-Mg}} = (X_{\text{Fs}}/X_{\text{En}})^{\text{A}}(X_{\text{En}}/X_{\text{Fs}})^{\text{Z}}$, where Z = Opx, Ptg, Ol, or ferrobustamite. K_{WB} is the "activity ratio" for Mg component [$a(\text{Aug})/a(\text{Opx or Ptg})$] as defined by Wood & Banno (1973) and used by Wells (1977). T_{WB} = temperature calculated from Eq. (27), Wood & Banno (1973, p.119). T_{W} = temperature calculated from Eq. (5) of Wells (1977). T_{W} values in () are for Aug-Ptg pairs (see text).*Range in values shows uncertainty of $\pm 1.5 X_{\text{wo}}$ for preferred $K_{\text{D}}^{\text{Fe-Mg}}$.

**First number is preferred value; uncertainties show ranges permitted by experimental brackets.

the similar point for 1100°C occurs at $Wo \sim 40$. Point n is at $X_{Fe} = 83$, $Wo = 50$, from Figure 2i.

At 1000°C, the field of ferrobustamite (B) occupies the area about Hd. The iron-rich limit q is from Lindsley & Munoz (1969). The solid-solution series may extend to some small contents of magnesium, shown schematically by the line $o-p$. Point o is the composition of ferrobustamite that grew in coexistence with the augite of composition n (data in Fig. 2i). The position of p [B(A,F,S)] was not determined, but it is estimated to have the same Fe/Mg ratio as o and the same content of Wo as q . The position of u [P(A,F,S)] is determined from the data in Figure 2e and 2f, as is v' . Point w' is inferred.

The lines $v-w$ and $v'-w'$ are the loci of composition points, taken from probe analyses, for Mg:Fe:Ca of olivines. Labeling of the lines F + S indicates the intersection of the tielines olivine + silica with the pyroxene quadrilateral plane in the system FeO–MgO–CaO–SiO₂.

DISCUSSION

Our major purpose in determining the pyroxene phase diagrams is to apply the results to geothermometry, with the recognition that "nonquadrilateral" components in natural pyroxenes may affect their phase relations or compositions. We compare our results first with those of other studies of synthetic pyroxenes, next, with Skaergaard and granulitic pyroxenes, and then with some empirical geothermometers.

Lindsley *et al.* (1974) determined the compositions of coexisting augite and orthopyroxene at 810°C and 15 kbar using many of the same starting materials employed in the present study. By analogy with the Di–En join and with natural occurrences, we would expect the two-pyroxene fields (O + A; A + P) for any fixed X_{Fe} to widen with decreasing temperature or with increasing pressure. However, the bands representing the A(O) and O(A) solvi at 900°C, 1 kbar overlap with those for 810°C, 15 kbar although there is permissive evidence to suggest that the two-phase field is marginally wider for the latter. The bulk-distribution coefficients K_D appear to be slightly higher (av. = 0.785) for the 900°C experiments than for those at 800°C (av. = 0.695: Table 2; Lindsley *et al.* 1974, Table 1) in keeping with the temperature differences.

Our (O + A) field at 1000°C, 1 atm is considerably wider than that shown for 1000°C, 15 kbar by Mori (1978, Fig. 5), but the discrepancy is not considered serious, because it results from one unreversed exsolution-experi-

ment by Mori (which, therefore, gives only a *minimum* width for that field).

Distribution coefficients (K_D) are listed in Table 2 to show bulk Fe–Mg partitioning between augite and the other phases. The values for augite–orthopyroxene at 900°C are higher than those calculated by Kretz (1963) and by Davidson (1968) for coexisting pairs from granulite-facies rocks, but the width of the two-pyroxene fields for the latter is considerably greater, in keeping with their lower temperatures of formation. The scatter in our K_D values (0.73 to 0.81) is interpreted as an indication of the error in assigning values from the limits of the reaction arrows in Figure 3.

Comparison of our experimental results with the compositions of Skaergaard pyroxene is not straightforward. All but the most magnesium-rich Skaergaard augites coexist with pigeonite rather than with orthopyroxene (Brown & Vincent 1963). Nevertheless, we can view the Skaergaard augite solvus ($15 < X_{Fe}^A < 45$) as saturated with some low-Ca pyroxene. This solvus crosses our 900 and 1000° solvi, with the more magnesian (and therefore higher-temperature) natural augites having *higher* Ca contents and the less magnesian ones having *lower* Ca contents. That the Skaergaard pyroxenes formed at higher temperatures than 900–1000°C is attested both by petrological arguments and by the low X_{Fe}^P value for the earliest pigeonite: a value X_{Fe}^P between 30 and 35 implies temperatures in the range 1150–1130°C (Ross & Huebner 1979). The apparently anomalous Ca values of the magnesium-rich Skaergaard augites probably reflect their content of Al₂O₃ (up to 3.22 wt. %): correction for a CaAlSiAlO₆ component would considerably decrease the effective Wo content of these augites. Our synthetic augites clearly must not be compared directly with natural ones containing Al₂O₃ in amounts greater than approximately 2 wt. %.

We have used our experimental data to determine apparent equilibrium "temperatures" for coexisting augite and orthopyroxene (Table 2) using the two-pyroxene thermometers of Wood & Banno (1973) and Wells (1977). The experimental uncertainty in the Wo contents of our augites introduces a variation of 30–90°C in the calculated temperatures, but some trends are clear. Neither thermometer predicts the experimental data well, and both are most in error for the most Mg-rich pyroxenes, with apparent temperatures for $X_{Fe} = 10$ that are too high by 187–258°C (Wood & Banno) and by 130–223°C (Wells). The discrepancy diminishes with increasing bulk X_{Fe} : the Wood–Banno thermometer gives temperatures that are too low (for

the 900° experiments) at bulk $X_{Fe} = 50-60$, whereas that of Wells always gives temperatures that are too high. It seems that neither geothermometer is valid for pure Ca-Mg-Fe pyroxenes at 900°C. Because both thermometers have been widely used, it is worth considering possible sources of the discrepancy. Both the Wood & Banno (1973) and Wells (1977) thermometers employ the temperature dependence of the reaction.

$Mg_2Si_2O_6$ (Cpx) = $Mg_2Si_2O_6$ (Opx) (A) with explicit corrections for the effect of Fe and implicit ones for the effects of Al, Ti, etc. A basic assumption of their models is that the Opx and Cpx solutions on the Di-En join are ideal. Effects of minor deviations from ideality are considered to be incorporated within the terms expressing the Gibbs free energy of reaction (A), and to be negligible within the error limits of the empirical calibration. Table 3 compares the reaction constants as deduced by Wells for reaction (A) with more recent models that permit nonideality in the Opx and Cpx solutions. The large differences (> 24 kJ) suggest that effects of nonideality should be treated explicitly.

The effect of pressure was also considered to be negligible for the range 1 bar to 40 kbar by Wells (1977, p. 131). The $P\Delta V$ term gives $\Delta T_p = 0.5$ °/kbar (Wells 1980, pers. comm.). There is also a small effect of $W\Delta V$ (Lindsley *et al.* 1981) that would be enhanced by any additional components that enhance the non-ideality. These corrections would have only a small effect on the calibration of the thermometer.

The correction term employed by Wells (1977) for Fe content (X_{Fe}^{Opx}) appears, in his Figure 3, to be dominated by results from two sets of experiments, those of Ross *et al.* (1973) and of Smith (1972). Ross *et al.* (1973) explicitly stated that their compositions are *semi-quantitative*; furthermore, they dealt with augite-pigeonite relations, although Wells (pers. comm. 1980) "... used Saxena's (1976) approach to obtain equilibrium augite-orthopyroxene compositions from the experiments of Ross *et al.* (1973)." The data of Smith (1972) pertain to

$P = 15$ kbar, bulk composition $X_{Fe} = 85$. The compositions of the A-O solvus pair at 875°C (used by Wells 1977, Fig. 3) are poorly bracketed, and the composition of the closest clinopyroxene brackets is known, by X-ray determination, only to the extent of the Ca content.

The effect of variable contents of Al on the thermometer equations of Wood & Banno (1973) and Wells (1977) is implicit in $\ln K$; Wells (1977, p. 133) pointed out that this is empirically satisfactory with regard to his data on Di-En. However, the deviation of our clinopyroxene compositions from the Skaergaard trend (above) and the scatter in the low-iron data points in Figure 3 of Wells (1977, p. 134) suggest that it also needs an explicit correction.

Our results should be of use in the calibration of a new empirical thermometer, as well as in the development of rigorous thermodynamic models for Ca-Mg-Fe pyroxenes.

ACKNOWLEDGEMENTS

This work was supported by grants from the Natural Sciences and Engineering Research Council of Canada (A2688 to Turnock) and the U. S. National Science Foundation (EAR-7622129 to Lindsley). We appreciate constructive comments by J.S. Huebner, F.C. Hawthorne, P. R. A. Wells and an anonymous reviewer.

REFERENCES

- ATLAS, L. (1952): The polymorphism of $MgSiO_3$ and solid-state equilibria in the system $MgSiO_3$ - $CaMgSi_2O_6$. *J. Geol.* **60**, 125-147.
- BONNICHSEN, B. (1969): Metamorphic pyroxenes and amphiboles in the Biwabik Iron Formation, Dunka River area, Minnesota. *Mineral. Soc. Amer. Spec. Pap.* **2**, 217-239.
- BOWEN, N.L. & SCHAIRER, J.F. (1935): The system MgO - FeO - SiO_2 . *Amer. J. Sci.* **229**, 151-217.
- , ——— & POSNJAK, E. (1933): The system CaO - FeO - SiO_2 . *Amer. J. Sci.* **226**, 193-284.
- BOYD, F.R. (1973): A pyroxene geotherm. *Geochim. Cosmochim. Acta* **37**, 2533-2546.
- & SCHAIRER, J.F. (1964): The system $MgSiO_3$ - $CaMgSi_2O_6$. *J. Petrology* **5**, 275-309.
- BROWN, G.M. & VINCENT, E.A. (1963): Pyroxenes from the late stages of fractionation of the Skaergaard intrusion, east Greenland. *J. Petrology* **4**, 175-197.
- DAVIDSON, L.R. (1968): Variation in ferrous iron-magnesium distribution coefficients of metamorphic pyroxenes from Quairading, western Australia. *Contr. Mineral. Petrology* **19**, 239-259.

TABLE 3. THERMODYNAMIC CONSTANTS FOR THE REACTION $Mg_2Si_2O_6$ (Cpx) = $Mg_2Si_2O_6$ (Opx) FOR THE DI-EN JOIN

Reference	H_A^0 (kJ)	S_A^0 (kJ/K)	$G_A^0(900^\circ\text{C})$ (kJ)
Wells (1977)	61.0	0.028	28.15
Holland <i>et al.</i> (1979)	6.8	0.0028	3.52
Lindsley <i>et al.</i> (1981)	3.6	0.0019	1.41*

* ΔG_A^0 value includes pressure effect at 1 kb ($\Delta V_A^0 = 0.036$ kJ/kb).

- DAVIS, B.T.C. & BOYD, F.R. (1966): The join $Mg_2Si_2O_6$ - $CaMgSi_2O_6$ at 30 kilobars pressure and its application to pyroxenes from kimberlites. *J. Geophys. Res.* **71**, 3567-3576.
- HESS, H.H. (1941): Pyroxenes of common mafic magmas. *Amer. Mineral.* **26**, 515-535, 573-594.
- HOLLAND, T.J.B., NAVROTSKY, A. & NEWTON, R.C. (1979): Thermodynamic parameters of $CaMgSi_2O_6$ - $Mg_2Si_2O_6$ pyroxenes based on regular solution and cooperative disordering models. *Contr. Mineral. Petrology* **69**, 337-344.
- HUEBNER, J.S. (1971): Buffering techniques for hydrostatic systems at elevated pressures. In *Research Techniques for High Pressure and High Temperature* (G.C. Ulmer, ed.). Springer-Verlag, New York.
- & TURNOCK, A.C. (1980): The melting relations at 1 bar of pyroxenes composed largely of Ca-, Mg-, and Fe-bearing components. *Amer. Mineral.* **65**, 225-271.
- KRETZ, R. (1963): Distribution of magnesium and iron between orthopyroxene and calcic pyroxene in natural mineral assemblages. *J. Geol.* **71**, 773-785.
- LINDSLEY, D.H. & DIXON, S.A. (1976): Diopside-enstatite equilibria at 850° to 1400°C, 5 to 35 kb. *Amer. J. Sci.* **276**, 1285-1301.
- , GROVER, J.E. & DAVIDSON, P.M. (1981): The thermodynamics of the $Mg_2Si_2O_6$ - $CaMgSi_2O_6$ join: a review and a new model. In *Advances in Physical Geochemistry 1* (S.K. Saxena, ed.). Springer-Verlag, New York.
- , KING, H.E. & TURNOCK, A.C. (1974): Compositions of synthetic augite and hypersthene coexisting at 810°C: applications to pyroxenes from Lunar Highland rocks. *Geophys. Res. Lett.* **3**, 134-136.
- & MUNOZ, J.L. (1969): Subsolidus relations along the join hedenbergite-ferrosilite. *Amer. J. Sci.* **267-A** (Schairer vol.), 295-324.
- MORI, T. (1978): Experimental study of pyroxene equilibria in the system CaO - MgO - FeO - SiO_2 . *J. Petrology* **19**, 45-65.
- PHILPOTTS, A.R. (1966): Origin of the anorthosite-mangerite rocks in southern Quebec. *J. Petrology* **7**, 1-64.
- PODPORA, C. & LINDSLEY, D.H. (1979): Fe-rich pigeonites: minimum temperatures of stability in the Ca-Mg-Fe quadrilateral. *Amer. Geophys. Union Trans.* **60**, 420-421 (abstr.).
- ROSS, M. & HUEBNER, J.S. (1979): Temperature-composition relationships between naturally occurring augite, pigeonite, and orthopyroxene at one bar pressure. *Amer. Mineral.* **64**, 1133-1155.
- , ——— & DOWTY, E. (1973): Delineation of the one atmosphere augite-pigeonite miscibility gap for pyroxenes from lunar basalt 12021. *Amer. Mineral.* **58**, 619-635.
- SAXENA, S.K. (1976): Two pyroxene geothermometer: a model with an approximate solution. *Amer. Mineral.* **61**, 643-652.
- SIMMONS, E.C., LINDSLEY, D.H. & PAPIKE, J.J. (1974): Phase relations and crystallization sequence in a contact-metamorphosed rock from the Gunflint Iron Formation, Minnesota. *J. Petrology* **15**, 539-565.
- SMITH, D. (1972): Stability of iron-rich pyroxene in the system $CaSiO_3$ - $FeSiO_3$ - $MgSiO_3$. *Amer. Mineral.* **57**, 1413-1428.
- TURNOCK, A.C., LINDSLEY, D.H. & GROVER, J.E. (1973): Synthesis and unit-cell parameters of Ca-Mg-Fe pyroxenes. *Amer. Mineral.* **58**, 50-59.
- WELLS, P.R.A. (1977): Pyroxene thermometry in simple and complex systems. *Contr. Mineral. Petrology* **62**, 129-139.
- WOOD, B.J. & BANNO, S. (1973): Garnet-orthopyroxene and orthopyroxene-clinopyroxene relationships in simple and complex systems. *Contr. Mineral. Petrology* **42**, 109-124.

Received July 1980, revised manuscript accepted December 1980.